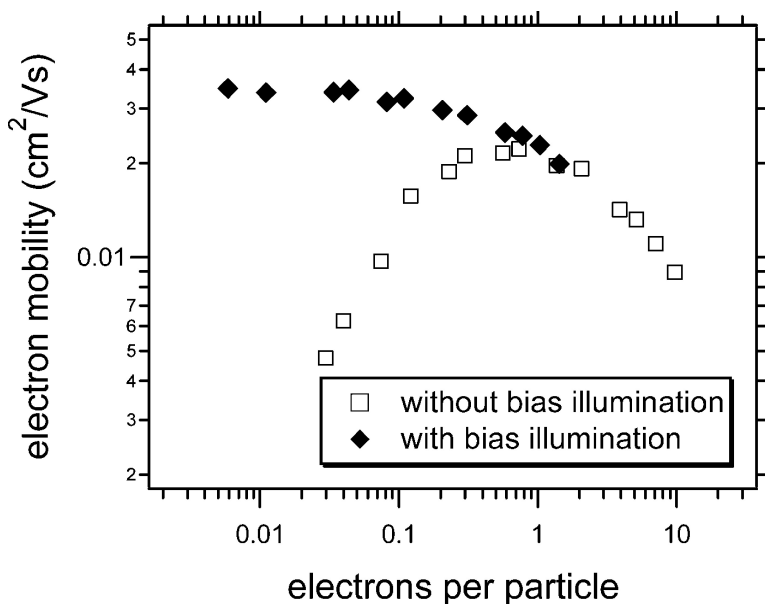Article

Electrodeless Determination of the Trap Density, Decay Kinetics, and Charge Separation Efficiency of Dye-Sensitized Nanocrystalline TiO

Jessica E. Kroeze, Tom J. Savenije, and John M. Warman

More About This Article

Additional resources and features associated with this article are available within the HTML version:

- Supporting Information
- Links to the 13 articles that cite this article, as of the time of this article download
- Access to high resolution figures
- Links to articles and content related to this article
- Copyright permission to reproduce figures and/or text from this article

View the Full Text HTML

J|A|C|S

A R T I C L E S

Electrodeless Determination of the Trap Density, Decay Kinetics, and Charge Separation Efficiency of Dye-Sensitized Nanocrystalline TiO$_2$

Jessica E. Kroeze,* Tom J. Savenije, and John M. Warman

Contribution from the Radiation Chemistry Department, IRI, Delft University of Technology, Mekelweg 15, 2629 JB Delft, The Netherlands

Received October 29, 2003; E-mail: kroeze@iri.tudelft.nl

Abstract: We have studied photoinduced charge separation in a bare, 3.4 μm thick layer of nanocrystalline ("nc") anatase TiO$_2$ and an nc-TiO$_2$ layer coated with free-base 5,10,15,20-tetrakis(4-carboxyphenyl) porphyrin (H$_2$TPPC) using the electrodeless flash-photolysis time-resolved microwave-conductivity technique (FP-TRMC). Photoconductivity transients, resulting from the formation of mobile, conduction band electrons in the semiconductor have been measured on excitation with 3 ns pulses of UV (300 nm) and visible (410–700 nm) light. The product of the yield of formation of mobile charge carriers, ϕ, and the sum of their mobilities, $\Sigma\mu$, has been determined from the maximum conductivity for light intensities varying from ~10^{12} to ~10^{16} photons/cm^2/pulse. For the bare nc-TiO$_2$ layer at 300 nm and the coated layer at all wavelengths, $\phi\Sigma\mu$ initially increased with increasing intensity, reached a maximum, and eventually decreased at high intensities. The initial increase is attributed to the gradual filling of (surface) electron trapping sites. This effect was absent when the samples were continuously illuminated with background irradiation at 300 nm with an intensity of 6×10^{13} photons/cm^2/s (40 μW/cm^2), thereby presaturating the trapping sites prior to the laser pulse. The trap-free mobility of electrons within these 9 nm nanoparticles is estimated to be 0.034 cm^2/Vs at 9 GHz. The eventual decrease in $\phi\Sigma\mu$ at intensities corresponding to an electron occupancy of more than one electron per particle is unaffected by background illumination, and is attributed to a decrease in μ due to electron–electron interactions within the semiconductor particles. The photoconductivity action spectrum of the coated nc-TiO$_2$ layer closely followed the photon attenuation spectrum in the visible of the porphyrin, with a charge separation efficiency per absorbed photon of 18% at the Soret band maximum. The after-pulse decay of the photoconductivity showed a power law behavior over a time scale of nanoseconds to several hundreds of microseconds, which is attributed to multiple trapping and detrapping events at chemical or physical defects within the semiconductor matrix.

1. Introduction

The application of organic antenna molecules for the sensitization of wide-band gap inorganic semiconductors for applications in photovoltaic devices has attracted much attention during the past decades.[1–3] In these devices, the absorption of visible light results initially in the creation of neutral photoexcitations within the organic moiety, which reach the interface with the semiconductor through exciton diffusion. At the interface, electron injection into the conduction band of the semiconductor occurs. Subsequently, the resulting charge carriers can diffuse away from the interface and be collected at the electrodes.

Key factors governing the overall efficiency of such a photovoltaic device are the wavelength dependence of interfacial charge separation (the 'action spectrum'), the intensity dependence of charge carrier generation and the exciton diffusion length. The determination of these parameters from photovoltaic measurements may be complicated by factors such as exciton deactivation at the cathode, nonohmic electrode contacts, filter effects, and pinhole defects in the photoactive layers. These complications can be surmounted by using the flash-photolysis time-resolved microwave conductivity (FP-TRMC) technique to probe the change in conductivity on photoexcitation of inorganic-semiconductor/organic-antenna layers. In this method, no electrical contacts are necessary and the change in conductivity within the sample is directly related to the amount of mobile electrons created in the conduction band of the semiconductor.[4]

We have recently used FP-TRMC to investigate quantitatively photoinduced charge separation in a bilayer consisting of a 60 nm film of free base 5,10,15,20-tetrakis(4-carboxyphenyl) porphyrin (H$_2$TPPC) spin-coated onto a smooth 80 nm thick layer of anatase TiO$_2$.[5] It was found that electron injection occurs from the first singlet excited state, S$_1$, of the porphyrin with an incident-photon-to-charge-separation efficiency (IPCSE) of only

(1) Giraudeau, A.; Fan, F.-R. F.; Bard, A. J. *J. Am. Chem. Soc.* **1980**, *102*, 5137−5142.
(2) Hagfeldt, A.; Grätzel, M. *Chem. Rev.* **1995**, *95*, 49−68.
(3) Nazeeruddin, M. K.; Kay, A.; Rodicio, I.; Humphrybaker, R.; Muller, E.; Liska, P.; Vlachopoulos, N.; Grätzel, M. *J. Am. Chem. Soc.* **1993**, *115*, 6382−6390.
(4) Savenije, T. J.; De Haas, M. P.; Warman, J. M. *Z. Phys. Chemie-Int. J. Res. Phys. Chem. Chem. Phys.* **1999**, *212*, 201−206.
(5) Kroeze, J. E.; Savenije, T. J.; Warman, J. M. *J. Photochem. Photobiol. A-Chem.* **2002**, *148*, 49−55.

0.8% at the Soret band maximum. This indicates that efficient electron injection occurs only from porphyrin molecules within the first 5 to 10 Å from the interface, corresponding to at most two monolayers. Apparently, diffusion of S_1 excitons from more distant regions of the porphyrin layer to the interface plays no significant role, thus limiting the efficiency of such a bilayer photovoltaic device.

Ways of overcoming the poor charge separation efficiencies associated with the short exciton diffusion length of organic sensitizer layers have been found in the application of porous nanocrystalline TiO₂ films.[6,7] These films consist of nanometer-sized crystallites sintered together into a porous conducting network, providing close to 1000-fold larger interface for charge separation. Unfortunately, the polycrystalline nature results in a large number of trap sites at grain boundaries and the inorganic/organic interface. These sites, which have been assigned to oxygen deficiencies and/or absorbed species, are energetically located below the TiO₂ conduction band with a distribution of energy levels that is usually assumed to be exponential,[8,9] although Wang and co-workers have suggested a more Gaussian-shaped distribution.[10]

Because of the absence of a significant electrical potential gradient in the major part of the nc-TiO₂ film,[11] bulk electron transport is believed to proceed by electron diffusion through the sintered nanoparticulate matrix.[12,13] Intensity modulated photocurrent spectroscopy (IMPS),[14−16] intensity modulated photovoltage spectroscopy (IMVS)[17] and time-of-flight (TOF)[18−20] and junction recovery[21] studies, as well as theoretical investigations[22,23] have shown that the time constants for electron diffusion strongly depend on light intensity. In all cases, it was concluded that *interparticle* electron diffusion in nanocrystalline TiO₂ is governed by electron trapping and detrapping events in intraband defect states present at high density on the surface of the particles or at grain boundaries between particles. Therefore, charge carrier transport in nanocrystalline TiO₂ is most often described in terms of an 'effective' diffusion coefficient D_{eff}, which strongly depends on the illumination intensity. D_{eff} values ranging between 10^{-8} cm² s⁻¹ at low intensities to 10^{-4} cm² s⁻¹ at high intensities have been reported.[16,19−21,24] In the aforementioned experimental and theoretical investigations, the TiO₂ matrix is treated as an effective medium, without paying particular attention to film morphology and grain connectivity. Recently, two studies have appeared demonstrating that also the network geometry[25] and grain morphology[26] have a notable effect on the electron transport dynamics. The former work is a both experimental and theoretical work illustrating that increasing the film porosity leads to a downward shift of the particle coordination number distribution, resulting in more tortuous and slower electron transport.[25] The latter work presents Monte Carlo simulations and analytical solutions to the continuity equation, demonstrating that the size of the particle necks has a marked influence on D_{eff}.[26]

The majority of the experimental work cited above was carried out in the presence of an I^-/I_3^- containing redox electrolyte. Device characteristics were found to be highly dependent on, often inseparable, contributions from the electrolyte, the pH, the applied potential and the illumination intensity.[10,27,28] Since our microwave conductivity technique does not require the use of electrode layers and a (liquid) electrolyte, it enables the intrinsic properties of the TiO₂ matrix layer to be studied.

In this work, we present results of a quantitative investigation of photoinduced charge separation in a dry, bare film of nanocrystalline ('nc') TiO₂ (Solaronix "Ti−Nanoxide HT") and an H₂TPPC-coated nc-TiO₂ film using the FP-TRMC technique. H₂TPPC was chosen as a sensitizer, since it is highly soluble in ethanol/pyridine, and exhibits distinct absorption features in the 400−450 nm and 500−700 nm regions. Its carboxy groups are believed to provide an intimate contact of the macrocycle with the semiconductor surface,[29] although in a recent comparative study no differences in the sensitization efficiency between H₂TPPC and its carboxy-free analogue H₂TPP were found.[30]

The HOMO and LUMO energy levels of H₂TPPC[31] and the valence and conduction band positions of anatase TiO₂[2] are shown in Figure 1, together with the primary and secondary processes that may occur on optical excitation.

Photoconductivity transients resulting from the formation of mobile, conduction band electrons in the semiconductor were measured on pulsed excitation with UV (300 nm) and visible (410−700 nm) light. At 300 nm, electrons are formed directly by band gap excitation of the semiconductor, as indicated by process 1 in Figure 1. In the visible, electron formation results from interfacial electron injection from photoexcitations created in the porphyrin antenna layer (process 3 in Figure 1). The wavelength-dependent efficiency of charge separation was determined by relating the conductivity resulting from photo-absorption in the porphyrin layer on visible photoexcitation, to

(6) O'Regan, B.; Grätzel, M. *Nature* **1991**, *353*, 737−740.
(7) Kay, A.; Grätzel, M. *J. Phys. Chem.* **1993**, *97*, 6272−6277.
(8) van de Lagemaat, J.; Frank, A. J. *J. Phys. Chem. B* **2000**, *104*, 4292−4294.
(9) Nelson, J.; Haque, S. A.; Klug, D. R.; Durrant, J. R. *Phys. Rev. B* **2001**, *6320*, art. no 205321.
(10) Wang, H. L.; He, J. J.; Boschloo, G.; Lindstrom, H.; Hagfeldt, A.; Lindquist, S. E. *J. Phys. Chem. B* **2001**, *105*, 2529−2533.
(11) O'Regan, B.; Moser, J.; Anderson, M.; Grätzel, M. *J. Phys. Chem.* **1990**, *94*, 8720−8726.
(12) Södergren, S.; Hagfeldt, A.; Olsson, J.; Lindquist, S. E. *J. Phys. Chem.* **1994**, *98*, 5552−5556.
(13) Boschloo, G. K.; Goossens, A. *J. Phys. Chem.* **1996**, *100*, 19489−19494.
(14) de Jongh, P. E.; Vanmaekelbergh, D. *Phys. Rev. Lett.* **1996**, *77*, 3427−3430.
(15) de Jongh, P. E.; Vanmaekelbergh, D. *J. Phys. Chem. B* **1997**, *101*, 2716−2722.
(16) Dloczik, L.; Ileperuma, O.; Lauermann, I.; Peter, L. M.; Ponomarev, E. A.; Redmond, G.; Shaw, N. J.; Uhlendorf, I. *J. Phys. Chem. B* **1997**, *101*, 10281−10289.
(17) Schlichthörl, G.; Huang, S. Y.; Sprague, J.; Frank, A. J. *J. Phys. Chem. B* **1997**, *101*, 8141−8155.
(18) Cao, F.; Oskam, G.; Meyer, G. J.; Searson, P. C. *J. Phys. Chem.* **1996**, *100*, 17021−17027.
(19) Solbrand, A.; Lindstrom, H.; Rensmo, H.; Hagfeldt, A.; Lindquist, S. E.; Södergren, S. *J. Phys. Chem. B* **1997**, *101*, 2514−2518.
(20) Kopidakis, N.; Schiff, E. A.; Park, N. G.; van de Lagemaat, J.; Frank, A. J. *J. Phys. Chem. B* **2000**, *104*, 3930−3936.
(21) Könenkamp, R. *Phys. Rev. B* **2000**, *61*, 11 057−11 064.
(22) Bisquert, J.; Zaban, A.; Salvador, P. *J. Phys. Chem. B* **2002**, *106*, 8774−8782.
(23) Nelson, J. *Phys. Rev. B−Condens Matter* **1999**, *59*, 15 374−15 380.

(24) Cao, F.; Oskam, G.; Searson, P. C.; Stipkala, J. M.; Heimer, T. A.; Farzad, F.; Meyer, G. J. *J. Phys. Chem.* **1995**, *99*, 11 974−11 980.
(25) Benkstein, K. D.; Kopidakis, N.; van de Lagemaat, J.; Frank, A. J. *J. Phys. Chem. B* **2003**, *107*, 7759−7767.
(26) Cass, M. J.; Qiu, F. L.; Walker, A. B.; Fisher, A. C.; Peter, L. M. *J. Phys. Chem. B* **2003**, *107*, 113−119.
(27) Haque, S. A.; Tachibana, Y.; Willis, R. L.; Moser, J. E.; Grätzel, M.; Klug, D. R.; Durrant, J. R. *J. Phys. Chem. B* **2000**, *104*, 538−547.
(28) Tachibana, Y.; Haque, S. A.; Mercer, I. P.; Durrant, J. R.; Klug, D. R. *J. Phys. Chem. B* **2000**, *104*, 1198−1205.
(29) Cherian, S.; Wamser, C. C. *J. Phys. Chem. B* **2000**, *104*, 3624−3629.
(30) Kroeze, J. E.; Savenije, T. J.; Warman, J. M. *Proc. SPIE* **2003**, *4801*, 67−79.
(31) Vergeldt, F. J.; Koehorst, R. B. M.; Schaafsma, T. J.; Lambry, J.-C.; Martin, J.-L.; Johnson, D. G.; Wasielewski, M. R. *Chem. Phys. Lett.* **1991**, *182*, 107.
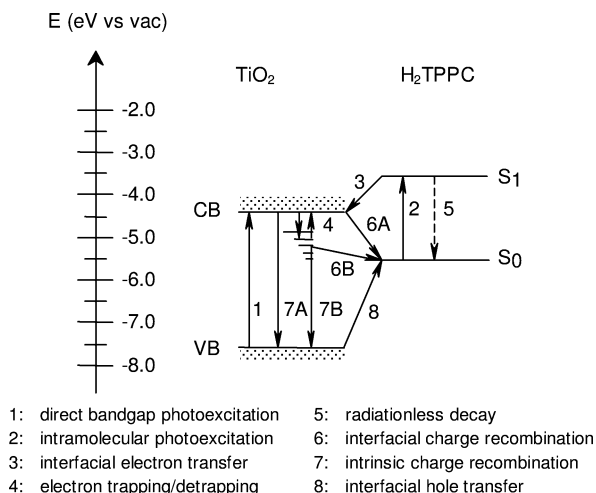
E (eV vs vac)

1: direct bandgap photoexcitation 5: radiationless decay
2: intramolecular photoexcitation 6: interfacial charge recombination
3: interfacial electron transfer 7: intrinsic charge recombination
4: electron trapping/detrapping 8: interfacial hole transfer

Figure 1. Schematic diagram of the energy levels of H$_2$TPPC in solution[29] and the valence and conduction band positions of anatase TiO$_2$,[2] together with the primary and secondary processes that may occur on optical excitation.

that observed by direct band-gap excitation using UV light. Measurements have been performed over a broad range of incident light intensities. In addition, the effect of continuous UV background illumination on the formation of mobile conduction band electrons was investigated.

2. Experimental Section

A. Sample Preparation. H$_2$TPPC was purchased from Porphyrin Products and used without further purification. Anatase TiO$_2$ was obtained as a colloidal suspension from Solaronix SA (Ti−Nanoxide HT, average particle size 9 nm, BET surface area 165 m^2/g). The preparation of nc-TiO$_2$ layers has been described in detail previously.[3] Briefly, to obtain nanocrystalline TiO$_2$ films of uniform thickness, a ca. 0.01 M solution of Ti(i-OPr)$_4$ in i-propanol was first spin-coated at 1800 rpm onto rectangular (12 × 25 mm^2), 1 mm thick quartz plates (Esco Products). These were dried at 450 °C in air, yielding a compact underlayer of TiO$_2$ adhering to the quartz substrate. The Solaronix TiO$_2$ paste was then spread onto this layer with a straight glass rod using Scotch tape as a spacer. After removal of the tape, the films were annealed in air for 12h at 450 °C, yielding transparent films. The film thickness was 3.4 μm as determined with a Veeco Dektak 8 Stylus step-profilometer. To adsorb the H$_2$TPPC, the freshly prepared film was immersed overnight in a 1 mM solution in pyridine/ethanol (1:1 by volume) at 50 °C. The unadsorbed dye was subsequently washed off with ethanol.

B. Optical Characterization. A Perkin-Elmer "Lambda 900" UV/Vis/NIR spectrophotometer fitted with an integrating sphere ("Labsphere") was used to measure the fraction of incident light reflected and transmitted by the sample, F_R and F_T, respectively. These values were used to determine the optical density, OD, which is defined by the relationships

$$F_T = (1 - F_R)10^{-OD} \tag{1}$$

$$= (1 - F_R)10^{-\epsilon cL} \tag{2}$$

In (2), ϵ is the extinction coefficient of the absorbing entity and c is its molar concentration.

An alternative parameter, frequently used when discussing thin layers of solid materials, is the linear absorption coefficient, α, defined by

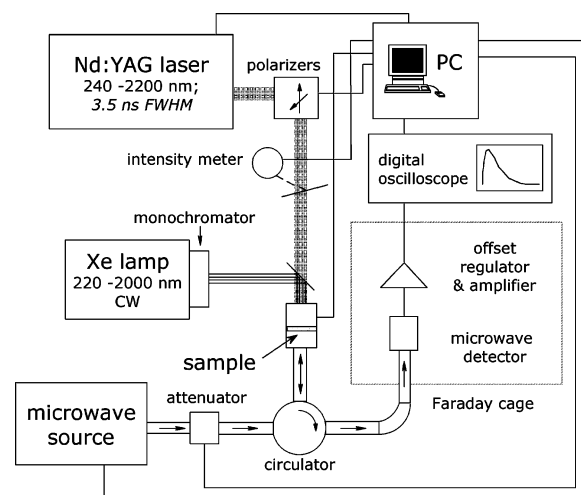$$F_T = (1 - F_R)e^{-\alpha L} \tag{3}$$

Figure 2. Schematic representation of the flash-photolysis time-resolved microwave conductivity setup, including the option of continuous bias illumination.

As can be seen, α is related to the optical density and ϵ by

$$\alpha = \frac{OD \ln 10}{L} = \epsilon c \ln 10 \tag{4}$$

A parameter which is often more relevant than either the absorption coefficient or the optical density when making comparisons with photoconductivity transients is the fraction of incident photons actually attenuated within the layer, F_A

$$F_A = 1 - (F_R + F_T) \tag{5}$$

The wavelength dependence of F_A is called here the "attenuation spectrum" to differentiate it from the "absorption spectrum", OD(λ).

C. Illumination Conditions. The samples were mounted in an X-band microwave cavity at a position corresponding to a maximum in the electric field strength of the standing wave pattern at resonance (for details, see ref 32). The sample could be illuminated via a grating in the copper end-plate of the cavity which was covered and vacuum sealed with a quartz window. The iris-coupling hole of the cavity was sealed with a polyimide foil. The cavity was attached to a vacuum line and the air was replaced by a mixture of 10% SF$_6$ in CO$_2$ at atmospheric pressure to scavenge any free electrons which might be ejected from the film by photoelectron emission.[33]

A schematic representation of the FP-TRMC setup is given in Figure 2. For photoexcitation in the visible, the third harmonic of a Q-switched Nd:YAG laser ("Infinity 15-30", Coherent) was used to pump an optical parametric oscillator (OPO) yielding 3 ns fwhm pulses continuously tunable from 410 to 700 nm. The beam was expanded using CaF$_2$ lenses to give a close to uniform intensity over a rectangular area A of ca. 1 × 2 cm^2, close to the cross-sectional dimensions of the cavity and the sample. The integrated incident laser intensity, I_0 (photons/cm^2/pulse), was monitored by deflecting a small percentage of the light to the pyroelectric sensor of a Labmaster power meter (Coherent). The intensity could be attenuated using a series of metal-coated neutral-density filters (Melles Griot). In this way I_0 could be varied by more than 4 orders of magnitude from ca. 10^{12} to 10^{16} photons/cm^2/pulse.

For studying the trap-saturation effects, the sample could be bias-illuminated with a continuous beam of 300 nm light from a Xenon lamp equipped with a Triax 190 monochromator. The intensity of this background irradiation was 6 × 10^{13} photons/cm^2/s (40 μW/cm^2). Above this intensity, the conductivity transients remained unchanged.

(32) De Haas, M. P.; Warman, J. M. *Chem. Phys.* **1982**, *73*, 35−53.
(33) Wegewijs, B. R.; Dicker, G.; Piris, J.; Garcia, A. A.; De Haas, M. P.; Warman, J. M. *Chem. Phys. Lett.* **2000**, *332*, 79−84.
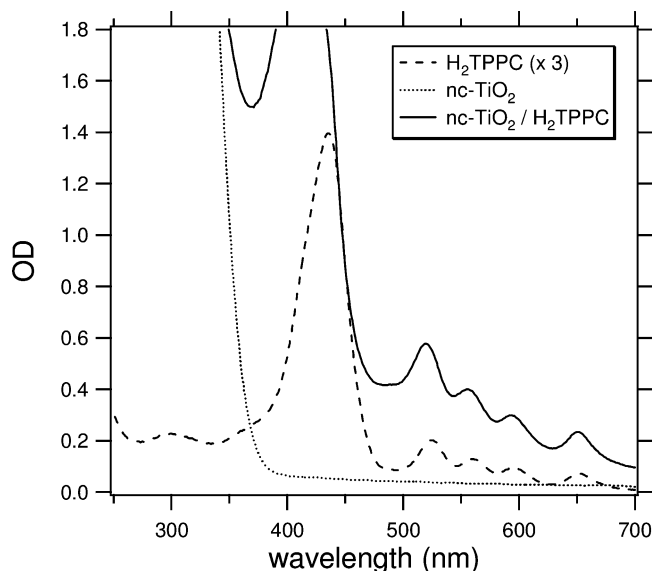
Figure 3. Absorption spectra of a 35 nm thick film of H₂TPPC alone (dashed line, multiplied by 3), a 3.4-μm thick uncoated nc-TiO₂ film (dotted line) and an H₂TPPC-coated nc-TiO₂ film (solid line), all on quartz substrates.

D. TRMC Measurements. Any photoinduced change in the conductance of the sample, ΔG, resulting from the formation of mobile charge carriers was monitored as a change in the power reflected by the cavity, $\Delta P/P$, using nanosecond time-response microwave circuitry and detection equipment described previously.[32] To monitor the conductivity change during and shortly after the laser pulse, a Tektronix TDS 680B digitizer was used. Long-lived transients were recorded with a Sony/Tektronix RTD 710A digitizer, which covered the time domain from tens of nanoseconds to milliseconds on a logarithmic time base. By combining the transients obtained with these two digitizers, the complete conductivity formation and decay upon photoexcitation could be monitored from nanoseconds to milliseconds. Several single-shot conductivity transients were averaged to improve the signal-to-noise ratio. The overall time-response of 18 ns was determined mainly by the loaded quality factor of the cavity, Q_L.

E. Data Analysis. The change in microwave power is related to the change in conductance of the irradiated film by

$$[\Delta P/P] = -K\,\Delta G \tag{6}$$

In eq 6, K is the sensitivity factor which can be derived from the resonance characteristics of the cavity and the dielectric properties of the medium; in the present work, $K = 19 \times 10^3$ S^{-1}. For a layer of thickness much smaller than the wavelength of the microwaves, as in the present case, ΔG is related to the conductivity at a depth z within the layer, $\Delta\sigma(z)$, by

$$\Delta G = \beta \int_0^L \Delta\sigma(z)\delta z \tag{7}$$

In eq 7, β is the ratio between the broad and narrow inner dimensions of the waveguide and is equal to 2.08 for the X-band waveguide used. Substituting in eq 7 for $\Delta\sigma(z) = eN(z)\sum\mu$, where e is the elementary charge, $N(z)$ the charge carrier pair concentration at depth z, and $\sum\mu$ is the sum of the charge carrier mobilities, results in

$$\Delta G = \beta e \sum \mu \int_0^L N(z)\delta z \tag{8}$$

If charge carriers are formed with an initial quantum yield ϕ_0 and no decay occurs during the pulse, then the integral in eq 8 is equal to $I_0F_A\phi_0$, and the conductance change, ΔG will be

$$\Delta G_0 = I_0 F_A \beta e \phi_0 \sum \mu \tag{9}$$

According to eq 9, the wavelength dependence of $\Delta G_0/I_0$ (the "photoconductivity action spectrum") should closely follow the attenuation spectrum, $F_A(\lambda)$, if ϕ_0 is wavelength independent. Rearrangement of eq 9 leads to an expression for the product of the quantum yield and mobility of charge carriers in terms of the experimentally measured parameters, ΔG, I_0, and F_A

$$\phi_0 \sum \mu = \frac{\Delta G_0/I_0}{F_A\beta e} \tag{10}$$

Since mobile charge carriers are formed during the pulse and eventually decay via charge recombination and/or trapping, ΔG will be time-dependent and the temporal form is referred to as a "photoconductivity transient", $\Delta G(t)$. If the decay occurs on a time scale much longer than the instrument response time, then the maximum value of $\Delta G(t)$, ΔG_{max}, will be equal to ΔG_0 and substitution in eq 10 will yield the true value of $\phi_0\Sigma\mu$. If, however, the decay of charge carriers occurs on a time scale comparable to the response time, the value of $\phi\Sigma\mu$ derived using ΔG_{max} in eq 10 will be a lower limit to $\phi_0\Sigma\mu$, i.e.

$$\phi \sum \mu = \frac{\Delta G_{max}/I_0}{F_A\beta e} \tag{11}$$

$$\leq \phi_0 \sum \mu \tag{12}$$

In studies of practical photovoltaic devices, the efficiency is usually related to the *incident* photon flux and given as the IPCE value; the "incident photon to current conversion efficiency". For more ready comparison with the present FP-TRMC measurements we have introduced the IPCSE parameter; the "incident photon to charge separation efficiency". This is related to the quantum yield per *absorbed* photon simply by IPCSE = ϕF_A.

3. Results and Discussion

Before presenting TRMC measurements of photon-induced charge separation we assess the optical properties of the samples investigated which provide information on the nature of the antenna layer and the depth profile of energy deposition within the films.

A. Optical Spectra and Penetration. 1. Absorption Spectra. The absorption spectra of a 35 nm thick layer of H₂TPPC alone on quartz and a 3.4 μm thick film of nc-TiO₂ with and without a coating of H₂TPPC are shown in Figure 3.

The characteristic porphyrin Soret band at 430 nm and the Q-bands in the 500 to 700 nm region dominate the absorption of the porphyrin-coated sample in the visible region. Below 350 nm however, direct band gap excitation of the TiO₂ component takes over as the most dominant photoexcitation process. The formation of electrons in the conduction band of the semiconductor can therefore be achieved almost exclusively either directly, by irradiation in the ultraviolet (process 1 in Figure 1), or indirectly, via excitation of the porphyrin in the visible followed by interfacial electron transfer (processes 2 and 3 in Figure 1). The TRMC results obtained in the UV and visible are therefore discussed separately in subsequent sections.

The optical density of the porphyrin absorption in the visible is a factor of close to 10 larger for the porphyrin-coated nc-TiO₂ layer (OD₅₂₀ = 0.58) than for the 34 nm thick porphyrin layer alone (OD₅₂₀ = 0.06). This demonstrates the greatly enhanced surface area available in the nanocrystalline film which results in an amount of porphyrin adsorbed equivalent to an

Table 1. Values of the Optical Absorption Coefficient α for Bare H$_2$TPPC and H$_2$TPPC-coated nc-TiO$_2$ Films at the Wavelengths Indicated[a]

sample	H$_2$TPPC		nc-TiO$_2$/H$_2$TPPC		
λ (nm)	α (10^6 m^{-1})	$\Lambda_{h\nu}$ (nm)	α (10^6 m^{-1})	$\Lambda_{h\nu}$ (nm)	F_R
300	5.1	196	6.1	163	0.16
430	32	31	3.4	293	0.11
520	4.4	227	0.39	2554	0.095

[a] Also given are the penetration depth of light, $\Lambda_{h\nu}$, and the fraction of reflected light, F_R, for H$_2$TPPC-coated nc-TiO$_2$ films.

H$_2$TPPC layer 340 nm thick. Of relevance to the present work is the actual thickness of the porphyrin coating on the individual, sintered TiO$_2$ particles within the film. This can be estimated by dividing the equivalent layer thickness of 340 nm by the surface amplification factor of the film, XS. This is the ratio of the total surface area available *within* the film to its cross-sectional area.

$$XS = L\rho_S S_w(1 - P) \qquad (13)$$

In eq 13, L is the film thickness, ρ_S is the density of the solid component, S_w is the surface area per unit weight, and P is the porosity of the film. For the nc-TiO$_2$ film studied in the present work $L = 3.4$ μm, $\rho_S = 3.84$ g/cm^3, $S_w = 165$ m^2/g and $P = 0.60$, which results in XS = 860. The average thickness of the porphyrin coating on the semiconductor particles is therefore ca. 0.4 nm. This amount of H$_2$TPPC corresponds to only approximately 15% of the free volume available within the nanoporous solid.

A thickness of 0.4 nm is much smaller than the value of 1.1 nm calculated for a monolayer of randomly orientated H$_2$TPPC molecules with a molecular weight of 790 and a density of ca. 1 g/cm^3. The saturation coverage of H$_2$TPPC on a sample of sintered TiO$_2$ with $S_w = 55$ m^2/g has been determined to be 0.85 μmole/m^2.[29] This corresponds to an average layer thickness of ca. 0.7 nm for a density of 1 g/cm^3 or a surface coverage of 2.0 nm^2 per molecule. This was interpreted as being due to a tendency for the disc-shaped H$_2$TPPC molecules to lie flat on the TiO$_2$ surface. The even smaller average thickness found for the present sample could be due to the fact that full saturation was not achieved within the time allowed for adsorption. The surface of the semiconductor particles may therefore be only partially covered with a monolayer of the porphyrin.

2. Depth Profile and Statistics of Photoexcitations. As will be shown later, the depth profile of photoexcitation within a film can play an important role in determining the overall efficiency of charge separation. The density of photons absorbed within a pulse at a depth z is given, to a first approximation, by

$$N_{h\nu}(z) = \alpha I(0)\exp[-\alpha z] \qquad (14)$$

In eq 14, $I(0)$ ($= [1 - F_R]I_0$) is the integrated number of photons per unit area penetrating the film. Since the absorption coefficient, α, is wavelength dependent, the depth profile can vary considerably when exciting in different regions of the absorption spectrum. This is illustrated in Table 1 where values of α are given for wavelengths of 300 nm (strong band gap absorption by TiO$_2$), 430 nm (Soret band of H$_2$TPPC), and 520 nm (strongest Q-band of H$_2$TPPC) for the porphyrin alone and for the porphyrin-coated nc-TiO$_2$ sample (see also Figure 3). Also given in the Table 1 are the values of the photon penetration

depth, $\Lambda_{h\nu} = 1/\alpha$, i.e. the depth within the film at which the intensity is reduced to 1/e or ca. 37% of its initial value. For the coated sample, $\Lambda_{h\nu}$ increases markedly from 163 to 293 to 2554 nm in going from 300 to 430 to 520 nm excitation. As a consequence, although more than 90% of the light will be absorbed within the first few hundred nanometers at 300 nm, at 520 nm photoexcitation will be much more uniform over the full film thickness. Such differences must be taken into account when comparing the effects of varying the incident intensity at different wavelengths.

The importance of the depth profile is accentuated in the present, nanocrystalline type of material because of the ultra-small size of the individual semiconductor particles. Because of this, the initial statistical distribution of photoexcitations between the particles must be taken into account. For a porous medium composed of particles of volume ΔV, the average number of photons absorbed per particle at a depth z is given by

$$\langle n_{h\nu}\rangle(z) = N_{h\nu}(z)\Delta V/(1 - P) \qquad (15)$$

The statistical distribution can be approximated by the Poisson relation, with $W(n)$ the probability of n photoexcitations in a given particle for an average value of $\langle n\rangle$

$$W(n) = \langle n\rangle^n \exp[-\langle n\rangle]/n! \qquad (16)$$

Because $\langle n_{h\nu}\rangle(z)$ is dependent on depth, we define for the purpose of subsequent discussion a characteristic value, $\langle n_{h\nu}\rangle$, as that pertaining at the depth at which half of the photons entering the layer have been absorbed, corresponding to the condition $\exp[-\alpha z] = 0.5$. From eqs 14 and 15 this results in

$$\langle n_{h\nu}\rangle = 0.5\alpha I(0)\Delta V/(1 - P) \qquad (17)$$

Replacing $I(0)$ by $I_0(1 - F_R)$ and ΔV by $36\pi/(\rho_S S_w)^3$ in eq 17 results in expression 18 for $\langle n_{h\nu}\rangle$ in terms of known or readily measurable parameters

$$\langle n_{h\nu}\rangle = 18\pi\alpha I_0(1 - F_R)/[(1 - P)(\rho_S S_w)^3] \qquad (18)$$

Taking the known values of P, ρ_S and S_w given in the previous section, we obtain for the nanocrystalline layers used in the present experiments

$$\langle n_{h\nu}\rangle = 5.6 \times 10^{-25}\alpha I_0(1 - F_R) \qquad (19)$$

with α in m^{-1} and I_0 in photons/m^2/pulse.

A parameter of interest is the light intensity for which, on average, one photon per particle is absorbed in the irradiated region. This is given by

$$I_0(\langle n_{h\nu}\rangle = 1) = 1.8 \times 10^{24}/\alpha(1 - F_R) \qquad (20)$$

According to Poisson statistics, for the condition $\langle n_{h\nu}\rangle = 1$, 42% of the those particles which have been photoexcited may have been multiply excited. A factor of 5 lower intensity is therefore required in order to achieve the condition that more than 90% of the photoexcited particles have absorbed only a single photon. Such considerations are of importance when considering the intensity dependence of the photoconductivity for the present type of nanocrystalline material.
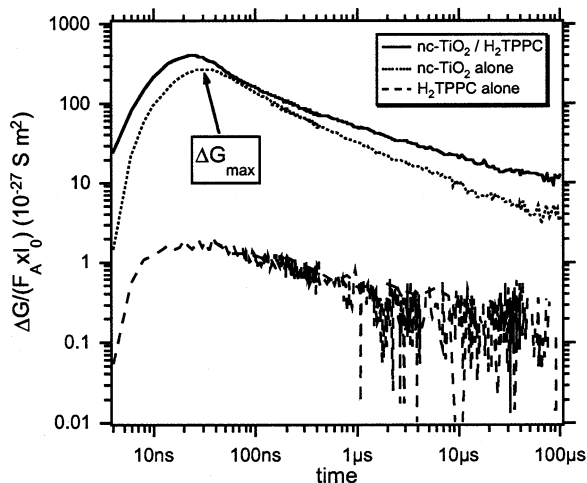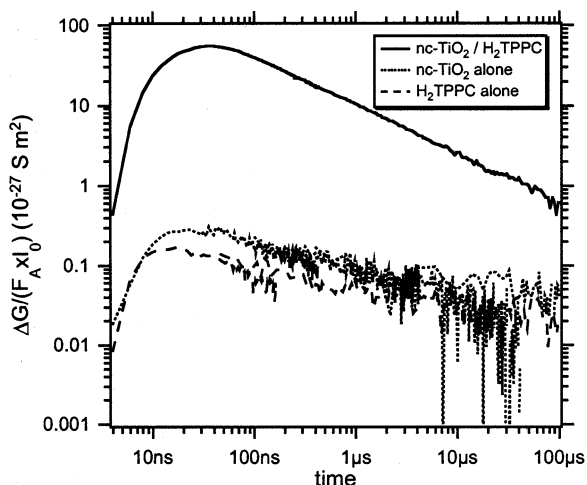
Figure 4. Intensity-normalized photoconductivity transients observed on excitation at 300 nm of an H₂TPPC film alone (dashed trace), a nc-TiO₂ film alone (dotted trace) and an H₂TPPC-coated nc-TiO₂ film (solid trace), all on quartz substrates. The pulse-integrated incident light intensities, I_0, were 3.3×10^{14} photons/cm², 3.5×10^{14} photons/cm² and 4.2×10^{14} photons/cm², respectively. The arrow indicates the position of ΔG_{max}, as explained in the Data analysis section.

Figure 5. Intensity-normalized photoconductivity transients observed on excitation at 520 nm of an H₂TPPC film alone (dashed trace), a nc-TiO₂ film alone (dotted trace) and an H₂TPPC-coated nc-TiO₂ film (solid trace), all on quartz substrates. The pulse-integrated incident light intensities, I_0, were 4.4×10^{15} photons/cm², 6.8×10^{15} photons/cm² and 3.2×10^{14} photons/cm², respectively.

B. Photoconductivity. In Figures 4 and 5 are shown examples of conductivity transients on photoexcitation at 300 and 520 nm for layers of H₂TPPC and nc-TiO₂ alone, and for the porphyrin-coated TiO₂ layer. At both wavelengths, the photoconductivity of the bare porphyrin layer is very small and close to the detection limit, as expected for this low dielectric constant organic material.

At 300 nm, absorption of the incident light in both the bare and porphyrin-coated TiO₂ samples is dominated (ca. 95% for the coated sample) by band-gap excitation of the semiconductor. The relatively large, and closely similar, photoconductivity transients observed are therefore attributed to the direct formation of mobile electrons within the anatase nanoparticles (process 1 in Figure 1).

At 520 nm, light is predominantly absorbed by the porphyrin, as shown by the spectra in Figure 3. Accordingly, only a small photoconductivity is found for the bare TiO₂ layer at this
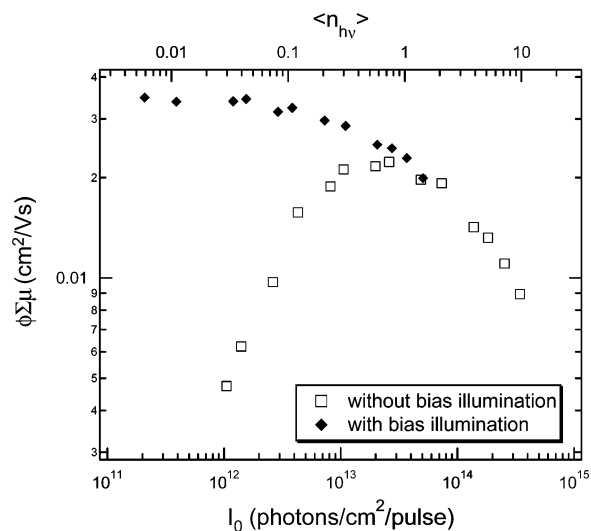

Figure 6. Intensity dependence of $\phi\Sigma\mu$ for a bare nc-TiO₂ film on pulsed illumination with 300 nm light, in the absence (open squares) and presence (closed diamonds) of 40 μW/cm² continuous, 300 nm, background illumination. The upper scale is the average number of photoexcitations per nanoparticle calculated using eq 19.

wavelength which is attributed to weak sub-bandgap excitation. The very much larger transient found for the coated sample at 520 nm is attributed to the indirect formation of mobile electrons within the semiconductor particles resulting from interfacial charge injection from excited states of the adsorbed porphyrin (process 3 in Figure 1). These results provide therefore clear-cut evidence for the sensitization of anatase TiO₂ by H₂TPPC. This is in agreement with results previously found by us in FP-TRMC studies of a double-layer of H₂TPPC spin-coated onto a smooth polycrystalline layer of anatase TiO₂,[5,34] as well as by others in steady-state[29,35] and time-resolved measurements.[28]

In what follows, we discuss in more detail the intensity dependence, wavelength dependence and after-pulse decay kinetics of the photoconductivity beginning with the nc-TiO₂ layer alone.

1. Bare nc-TiO₂, 300 nm Excitation. The nanocrystalline TiO₂ matrix in the present work consists of a sintered network of anatase crystallites of average diameter, d, equal to ca. 9 nm, corresponding to approximately 10 000 TiO₂ molecular units. Photoexcitation at 300 nm is expected to result in a direct band gap transition and the formation, initially, of electron–hole pairs within the individual crystallites with a quantum efficiency close to unity. Because of the ultrahigh frequency of the electric field oscillations in the present detection technique, the mobility of charge carriers within the organized domains of a sample should contribute mainly to the value of $\phi\Sigma\mu$ determined from the maximum conductivity. In the absence of trapping and/or recombination of carriers within the pulse, the value of $\phi\Sigma\mu$ should therefore be independent of light intensity and equal to the sum of the electron and hole mobilities within the bulk of the crystalline particles, i.e. $\phi\Sigma\mu \approx [\mu(-)_p + \mu(+)_p]$. However, as can be seen in Figure 6, the value of $\phi\Sigma\mu$ (open squares) in fact increases markedly with increasing intensity initially. This contrasts with the constant low-intensity behavior

(34) Kroeze, J. E.; Savenije, T. J.; Warman, J. M. *Adv. Mater.* **2002**, *14*, 1760–1763.
(35) Ma, T. L.; Inoue, K.; Noma, H.; Yao, K.; Abe, E. *J. Photochem. Photobiol. A-Chem.* **2002**, *152*, 207–212.

found for smooth, polycrystalline layers of anatase in previous FP-TRMC studies.[4]

The present behavior is reminiscent of the increase with intensity of the bulk diffusion coefficient of electrons, $D(-)_b$, within similar nanocrystalline TiO_2 layers found in previous DC measurements.[16,19−21,24] This effect has been explained in terms of the equilibrium localization of electrons at (surface) trapping sites and the gradual filling of these traps as the intensity (total number of electrons formed) is increased.[36] We conclude that it is this equilibrium trapping process and its saturation that is also responsible for the initial increase in $\phi\sum\mu$ with intensity in the present experiments. The initial superlinear increase (up to 2×10^{13} photons/cm^2/pulse) of the photoconductance ΔG_{max} with intensity displays a power law behavior according to $\Delta G \propto I_0^\delta$ with $\delta = 1.5$, very close to previously published values of the dc photoconductivity dependence on illumination intensity.[37−39]

To verify the mechanism of equilibrium trapping we have carried out FP-TRMC measurements on the same sample in the presence of continuous, background UV illumination with light from a CW Xenon lamp. The dramatic effect of this bias illumination is shown in Figure 6. Under these bias conditions, the value of $\phi\sum\mu$ is seen to be much larger and remains almost constant at the lowest laser intensities used. This is in agreement with the trapping mechanism proposed, with the background radiation functioning to presaturate the trapping sites prior to the laser pulse.

The data for bias illumination shown in Figure 6 represent the maximum effect on $\phi\sum\mu$ that could be achieved on increasing the bias intensity. We consider therefore that the low-intensity, limiting value of $\phi\sum\mu$ of 0.034 cm^2/Vs corresponds to complete trap saturation and therefore provides a measure of the trap-free mobility of electrons within the anatase nanoparticles. This corresponds to an *intraparticle* electron diffusion coefficient, $D(-)_p$, of ca. 10^{-3} cm^2/s which is an order of magnitude larger than the value of ca. 10^{-4} cm^2/s found for $D(-)_b$ in DC measurements.[20] The lower value of $D(-)_b$ is not particularly surprising since, even under conditions of trap saturation, bulk diffusion will be mainly determined by the rate of particle-to-particle transfer of electrons rather than by their diffusive motion within the particles themselves.

The value of $D(-)_b$ is however relevant to the present measurements since it provides an estimate of the average time that an electron (trapped or free) resides on a given particle, τ_p, via the relationship for 3-dimensional diffusion

$$D(-)_b = d^2/6\tau_p \qquad (21)$$

The increase in $D(-)_b$ from ca. 10^{-8} to ca. 10^{-4} cm^2/s with increasing intensity found in DC experiments[20] corresponds therefore to electron residence times ranging from ca. 10 μs at the lowest intensity to ca. 1 ns at the highest, in close agreement with values reported previously.[25] This will be referred to later when the after-pulse decay of the photoconductivity is discussed.

The value of 0.034 cm^2/Vs given above for the intraparticle, trap-free electron mobility is much lower than the value of ca.

2 cm^2/Vs found using the present technique for smooth polycrystalline layers of anatase,[4] or for nonporous crystalline samples using other techniques.[40] It does however agree rather well with mobility values determined for powder samples of anatase nanoparticles using the pulse-radiolysis TRMC technique which were found to decrease from 1.4 to 0.05 cm^2/Vs as the average particle size decreased from ca. 100 to ca. 10 nm.[41]

This dependence of the (microwave) mobility on particle size can be understood in terms of the scattering of electrons at the particle surface. An approximate estimate of the time scale on which surface scattering occurs, τ_s, is given by the average time required to undergo a root-mean-square displacement equal to half the particle diameter via three-dimensional diffusion, i.e.

$$\tau_s \approx d^2/24D(-)_p \qquad (22)$$

If we take $D(-)_p = 0.05$ cm^2/s (corresponding to $\mu(-) = 2$ cm^2/Vs), characteristic of the bulk crystalline material, then τ_s for the present nanoparticles is calculated to be less than 1 ps. This is very much shorter than the ca. 100 ps reciprocal frequency of the microwaves used. Electrons will therefore undergo surface scattering many times during one oscillation of the microwave electric field, thus explaining the "low" effective mobility measured. Even taking for $D(-)_p$ a value of ca. 10^{-3} cm^2/s (corresponding to $\mu(-)_p = 0.034$ cm^2/Vs) as a lower limit in eq 22, an electron would undergo a close encounter with the surface of a nanoparticle approximately once every 30 picoseconds. This is much shorter than even the shortest residence time of ca. 1 ns given above, indicating that electrons will "see" the surface of a particle many times prior to undergoing transfer to a neighboring particle. It is apparent therefore why equilibrium surface trapping occurs on a time scale well within the nanosecond time-resolution of the present measurements. Furthermore, the effect of surface scattering is supported by the recent theoretical work of Cass et al.,[26] who demonstrated that the rate of interparticle diffusion considerably slows down if the size of particle necks is reduced, implying that electrons have a larger chance of becoming trapped at the surface.

As can be seen in Figure 6, the $\phi\sum\mu$ values, both with and without bias illumination, eventually decrease and approach each other at the highest intensities used. This gradual decrease could be due to either rapid, in-pulse charge recombination (reducing ϕ) or to electron−electron interactions within multiply occupied nanoparticles resulting in a reduction in the effective electron mobility. In view of this, it is of interest to plot the experimental data as a function of the average number of electrons formed per particle rather than simply the incident light intensity. For this purpose, the parameter $\langle n_{h\nu} \rangle$, derived using eq 19, is given as the upper *x*-axis in Figure 6.

Two aspects of this method of presentation are of interest. First, the data with bias illumination begin to decrease significantly as $\langle n_{h\nu} \rangle$ approaches 1, indicating that multiple photo-excitation events are the cause of the decrease at elevated intensities. As mentioned in the previous section, for the

(36) Könenkamp, R.; Henninger, R.; Hoyer, P. *J. Phys. Chem.* **1993**, *97*, 7328−7330.

(37) Hoyer, P.; Könenkamp, R. *Appl. Phys. Lett.* **1995**, *66*, 349−351.

(38) Peter, L. M.; Wijayantha, K. G. U. *Electrochem. Commun.* **1999**, *1*, 576−580.

(39) Anta, J. A.; Nelson, J.; Quirke, N. *Phys. Rev. B* **2002**, *65*, art. no. 125324.

(40) Forro, L.; Chauvet, O.; Emin, D.; Zuppiroli, L.; Berger, H.; Levy, F. *J. Appl. Phys.* **1994**, *75*, 633−635.

(41) Warman, J. M.; Dehaas, M. P.; Pichat, P.; Koster, T. P. M.; Vanderzou-wenassink, E. A.; Mackor, A.; Cooper, R. *Radiat. Phys. Chem.* **1991**, *37*, 433−442.
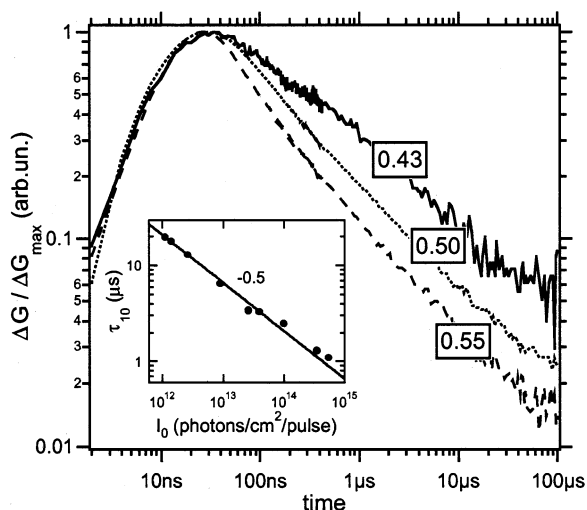
Figure 7. Intensity dependence of the photoconductivity decay on photoexcitation at 300 nm of a bare nc-TiO$_2$ film. The curves have been normalized to their respective maxima. The pulse-integrated incident light intensities, I_0, were 2.6×10^{12} photons/cm^2 (solid trace), 2.6×10^{13} photons/cm^2 (dotted trace) and 3.5×10^{14} photons/cm^2 (dashed trace), which corresponds to values for $\langle n_{h\nu} \rangle$ of 0.08, 0.8 and 10, respectively. Also given are the values of the exponent γ for the inverse power law decay tails. The inset shows the dependence of τ_{10} (see text for details) on I_0.

condition $\langle n_{h\nu} \rangle = 1$, approximately 40% of the particles that have been photoexcited will in fact be multiply excited according to Poisson statistics, eq 16. It is not possible, on the basis of the present data, to distinguish between charge recombination and electron–electron interactions as the underlying cause of the decrease. Second, the data with bias illumination approach closely those without bias in the region corresponding to $\langle n_{h\nu} \rangle \approx 1$. In other words, there is almost no effect of the bias illumination for conditions of laser pulse intensity corresponding to one or more photoexcitations per particle.

This, rather surprising, observation has been made by others in several quite different studies.[17,42–45] It suggests that the equilibrium localization phenomenon is based on a property of the whole nanoparticle rather than involving trapping at specific chemical or physical surface defects, which would have to possess a fortuitous concentration corresponding to one defect per particle. A fuller analysis of our intensity dependent data in a subsequent section may help to shed more light on this matter.

Until now, we have been concerned with the value of $\phi\Sigma\mu$ determined from the maximum photoconductivity and hence with processes which effect either the yield or mobility of mobile electrons on a time scale comparable with or shorter than the experimental time resolution of approximately 10 ns. We now turn to the eventual, after-pulse decay of the photoconductivity. This is illustrated for the bare TiO$_2$ layer with transients taken at different laser intensities in Figure 7.

As can be seen by the close to linear dependence in the log–log representation, the long-time decay tail is highly dispersive and follows an inverse power law behavior according to $\Delta G \propto t^{-\gamma}$, which is generally assumed to be characteristic of multiple

trapping with a broad energetic (exponential) distribution of electron traps.[9,39,44] A decrease in the decay time with increasing intensity is apparent, yielding values for γ of 0.43, 0.50 and 0.55 for incident intensities of 2.6×10^{12}, 2.6×10^{13} and 3.5×10^{14} photons/cm^2, respectively. The inset to Figure 7 shows the dependence of the time to decay to 10% of the maximum value, τ_{10}, on I_0 over the entire accessible intensity range. A power law dependence with slope −0.5 is observed, similar to earlier observations of the electron lifetime decay in both dry and dye-sensitized films.[38,39,46]

As mentioned previously, based on the bulk diffusion coefficient, the particle-to-particle electron-transfer time at high intensities, i.e., under conditions of trap saturation, occurs on a time scale of nanoseconds. During the course of microseconds, electrons will therefore visit many different particle sites. The after-pulse decay in the present experiments could therefore be attributed to localization of electrons in a region of the matrix other than that in which they were formed.

This localization could involve recombination with trapped hole sites or in the case of adsorbed H$_2$TPPC, with the dye radical cation or deep trapping at chemical or physical defects in the matrix. In this respect, it is important to distinguish between direct recombination of conduction band electrons and recombination via electron trap states, processes 7A/6A vs 7B/6B in Figure 1, respectively. The decrease in decay time with increasing intensity might be taken, at first sight, to favor the recombination pathway.[22,27] However, this is hard to reconcile with the evident similarity between the decay kinetics in the absence and presence of adsorbed sensitizer as displayed in Figures 4 and 5, respectively. We argue therefore, in the light of the previous discussion on the role of rapid equilibrium trapping in determining the rate of bulk diffusion, that it is the rate of diffusion through the matrix to deep defect sites that results in the intensity dependence observed. This would explain why the decay is slowest at the lowest intensity for which $\langle n_{h\nu} \rangle = 0.08$ and the equilibrium, intraparticle trapping process is not yet saturated.

It is worthwhile in this respect to recollect the recent work of Benkstein et al.,[25] which provides evidence for the dispersive decay at short times, i.e., up to $\sim 10^3\tau_p$, being determined by the fractality of the porous sample. Our observation that the decay kinetics of the bare nc-TiO$_2$ in the presence of trap-saturating bias illumination (data not shown) are still dispersive, are in support of this explanation. Therefore, future work addressing the microwave conductivity decay of nc-TiO$_2$ films of different porosities and particle sizes might reveal important information on the influence of fractality and the interparticle connectivity on electron transport dynamics.

2. H$_2$TPPC-Coated nc-TiO$_2$; 300 nm Excitation. As mentioned previously, the relative absorption coefficients of TiO$_2$ and the porphyrin at 300 nm are such that approximately 95% of the light will be absorbed by the semiconductor particles in the coated sample. The primary photon absorption process would therefore be expected to be closely similar to that for the bare TiO$_2$ layer, i.e., a band-gap transition within the bulk of the crystallites (process 1 in Figure 1). In agreement with this, the absolute magnitude and intensity dependence of $\phi\Sigma\mu$

(42) Duffy, N. W.; Peter, L. M.; Rajapakse, R. M. G.; Wijayantha, K. G. U. *J. Phys. Chem. B* **2000**, *104*, 8916–8919.
(43) Goossens, A.; van der Zanden, B.; Schoonman, J. *Chem. Phys. Lett.* **2000**, *331*, 1–6.
(44) van de Lagemaat, J.; Frank, A. J. *J. Phys. Chem. B* **2001**, *105*, 11 194–11 205.
(45) van 't Spijker, H.; Goossens, A. *Thin Solid Films* **2002**, *403*, 410–414.

(46) Schlichthörl, G.; Park, N. G.; Frank, A. J. *J. Phys. Chem. B* **1999**, *103*, 782–791.
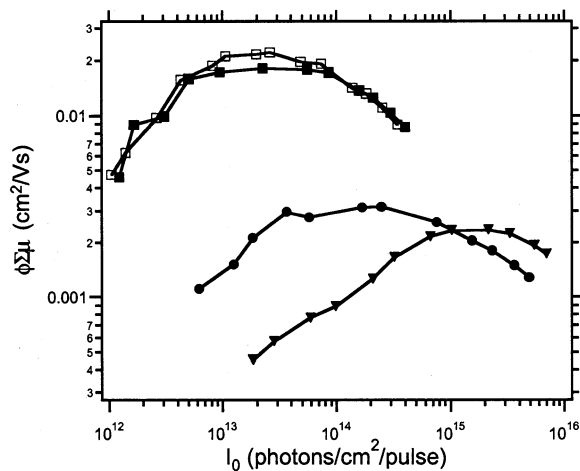
Figure 8. Intensity dependence of $\phi\Sigma\mu$ for a nc-TiO$_2$ film (open symbols) and an H$_2$TPPC-coated nc-TiO$_2$ film (closed symbols) on excitation at 300 nm (squares), 430 nm (circles) and 530 nm (triangles).

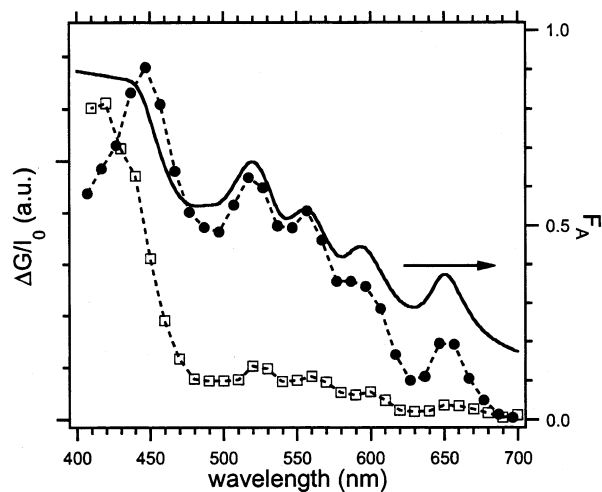**Figure 9.** Wavelength dependence ("action spectrum") of the incident intensity-normalized maximum photoconductance, $\Delta G_{max}/I_0$, for an H$_2$TPPC coated nc-TiO$_2$ film, with I_0 ca. 10^{15} photons/cm^2/pulse (solid circles) and 2×10^{13} (open squares) photons/cm^2/pulse. The full line represents the fraction F_A of incident photons absorbed by the film.

for the coated sample are almost identical to that for the bare sample, as shown in Figure 8.

The close similarity in the low-intensity region indicates that the adsorbed surface layer of porphyrin molecules has no significant influence on the equilibrium trapping process responsible for the increase in $\phi\Sigma\mu$ with intensity. This lends support to the conclusion reached in the previous section that electron localization is related to a property of the whole semiconductor particle, rather than to spurious chemical or physical surface defects since the latter would almost certainly be expected to be influenced by the presence of the adsorbant.

The fact that the decrease of $\phi\Sigma\mu$ in the high-intensity regime for the coated sample is also almost identical to that for the bare layer, lends support to the source of this effect being electron–electron interactions within the particles rather than the rapid, in-pulse recombination of electrons with (surface-trapped) holes. This argument is based on the expectation that the adsorbed porphyrin molecules should act as deep traps for positive charge thus drastically changing the nature of the recombination process.

The eventual, after-pulse decay of the conductivity in the high-intensity regime is also seen in Figure 4 to be similar to that for the bare sample, although somewhat slower at long times. In both cases, the time to decay to 10% of the maximum value is close to 3 μs. From the relative insensitivity of the decay kinetics to the presence of the porphyrin layer, we conclude that underlying process responsible most probably involves localization at deep traps intrinsic to the semiconductor matrix, rather than recombination with surface hole states (process 7 in Figure 1), which would be expected to be influenced by the presence of the adsorbant.

3. H$_2$TPPC-Coated nc-TiO$_2$; 410−700 nm Excitation. Light in the visible region of the spectrum is absorbed almost exclusively by the porphyrin component of the coated TiO$_2$ layer, as shown by the spectra in Figure 3. As mentioned previously, clear-cut evidence that photons absorbed by the porphyrin result in the formation of mobile electrons within the TiO$_2$ nanoparticles (process 3 in Figure 1) is provided in Figure 5 by the 2 orders of magnitude larger photoconductivity transient for the coated layer than for either the TiO$_2$ or H$_2$TPPC layers

alone, on irradiation at 520 nm. The semiconductor-sensitization or antenna function of the porphyrin is even more clearly demonstrated by the spectral dependence of the intensity-normalized photoconductance, $\Delta G/I_0$, shown in Figure 9. The conductivity action spectra display the same features, characteristic of the porphyrin Soret and Q-bands, that are present in the optical attenuation spectrum, $F_A(\lambda)$, which is shown in the same figure for comparison.

It is apparent in Figure 9 that the action spectra taken for two different incident intensities do not scale equally in the Soret and Q-band regions. The reason for this becomes apparent when the overall intensity dependences of $\phi\Sigma\mu$ monitored at 430 and 520 nm are compared, as in Figure 8. The results appear at first sight to be complex and very different for the two wavelengths, with $\phi\Sigma\mu$ largest for the Soret band at the lowest intensities and for the Q-band at the highest intensities. The general form of the $\phi\Sigma\mu$ dependence is however seen to be quite similar at both wavelengths in the log−log representation, and even resembles that found for (direct band-gap) excitation at 300 nm. At all three wavelengths, $\phi\Sigma\mu$ increases at the lowest intensities, reaches a maximum, and eventually decreases at the highest intensities. The intensity at which the maximum value of $\phi\Sigma\mu$ is reached shifts however from ca. 2.6×10^{13} to ca. 2.5×10^{14} to ca. 2.2×10^{15} photons/cm^2/pulse in going from 300 to 430 to 520 nm. In addition, the maximum value of $\phi\Sigma\mu$ reached is substantially lower for the two visible wavelengths than for 300 nm.

The results can be rationalized on the basis of the following: (a) the mobility and secondary interactions of electrons within the TiO$_2$ matrix are independent of whether they are formed directly by band-gap excitation or indirectly via electron injection from the antenna layer (processes 1 or 3 in Figure 1), (b) the quantum yield of electron formation, ϕ_e, is unity for direct band-gap excitation but lower for interfacial charge separation after photon absorption in the antenna layer, (c) the processes responsible for the intensity dependence of $\phi\Sigma\mu$ are dependent only on the average number of electrons formed per nanoparticle, $\langle n_{ep}\rangle$, which is related to the incident intensity and
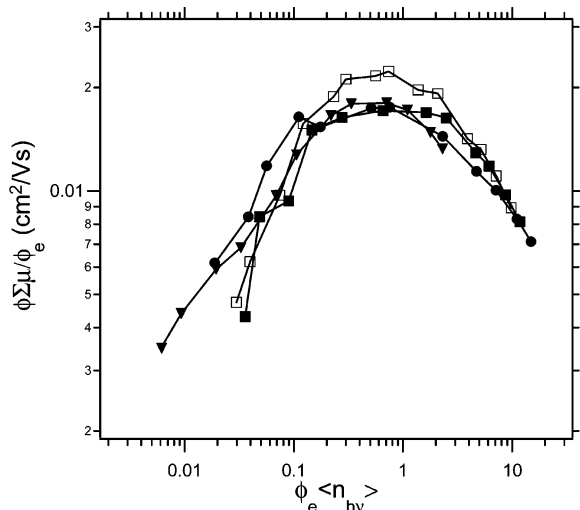
Figure 10. Dependence of $\phi\Sigma\mu/\phi_e$ on $\phi_e\langle n_{h\nu}\rangle$ for a nc-TiO₂ film (open symbols) and an H₂TPPC-coated nc-TiO₂ film (closed symbols) on excitation at 300 nm (circles), 430 nm (circles) and 530 nm (triangles). ϕ_e is the quantum yield for electron formation and $\langle n_{h\nu}\rangle$ is the average number of photons absorbed per nanoparticle (see text for clarification).

the absorption coefficient at a given wavelength by

$$\langle n_{ep}\rangle = \phi_e\langle n_{h\nu}\rangle$$

$$= 5.6 \times 10^{-25}\alpha I_0(1 - F_R)\phi_e \qquad (23)$$

The only unknown parameter in eq 23 is ϕ_e. This can however be estimated with reasonable accuracy from the ratio of the maximum value of $\phi\Sigma\mu$ for 430 and 520 nm irradiation to that found in the UV, yielding values of 0.18 and 0.13, respectively. The large shifts in the intensity dependent data can be seen to result in part from the lower ϕ_e values in the visible but mainly from the strong dependence on wavelength of the absorption coefficient (penetration depth) as shown in Table 1.

On the basis of the above, a plot of $\phi\Sigma\mu/\phi_e$ against $\phi_e\langle n_{h\nu}\rangle$ should result in a unified dependence of all of the data, as is shown to be the case in Figure 10. We emphasize that, apart from the value chosen for ϕ_e, all of the other parameters determining the x and y coordinates of the data points in Figure 10 are based on experimentally determined parameters.

From the good agreement between the data for direct, intraparticle electron formation in the UV and interfacial electron injection in the visible, we conclude that the processes responsible for the initial increase and eventual decrease in $\phi\Sigma\mu$ are unaffected by the presence of the antenna layer and, by inference, independent of the nature of the positive ion at the surface. This provides further support for the shallow trapping of electrons at low intensities being the result of a whole-particle property rather than localization at surface-defects. The agreement would also favor electron—electron interactions on multiple occupancy of particles, i.e., Coulombic repulsion in the present electrolyte-free environment, as the explanation of the decrease of $\phi\Sigma\mu$ at high intensities, rather than in-pulse charge recombination.

The rather low values of ϕ_e on visible excitation are somewhat surprising in view of the estimated average surface coverage of less than a single monolayer of porphyrin molecules. Interfacial charge separation following photoexcitation of dye molecules directly adsorbed on TiO₂ particles has been found

to occur on a time scale of picoseconds or less,[28] i.e. much shorter than the natural S₁ lifetime of several nanoseconds for an isolated H₂TPPC molecule. If indeed each H₂TPPC molecule were in intimate contact with the semiconductor surface in the coated sample, a quantum yield of close to unity would have been expected. In FP-TRMC experiments on H₂TPPC adsorbed on a smooth nonporous layer of anatase, we have shown that only the first and possible the second monolayers are active in charge separation.[5] We suggest three possible explanations for the low quantum yields observed: (a) an efficient radiationless decay pathway for S₁ exists in competition with interfacial charge separation, (b) a large fraction of the surface sites at which H₂TPPC molecules are adsorbed are "inactive", (c) H₂TPPC is not spread evenly over the available surface within the whole nanoporous layer but forms porphyrin-rich aggregates in which a large fraction of H₂TPPC molecules are distant from a semiconductor particle surface. At present, we are carrying out experiments using other antenna molecules in the hope that this provides further information that makes it possible to choose between these alternative explanations.

The after-pulse decay kinetics of the photoconductivity of the coated-layer on excitation in the visible are very similar to those found in the UV for either the coated or the uncoated sample. The transients obtained on excitation in the Q-band at 520 nm display disperse kinetic behavior with an inverse power dependence on time in the 100 ns to 100 μs time domain, as shown in Figure 5. The time taken to decay to 10% of the maximum value is approximately 3 μs, which is within the range from 1.1 to 20 μs found for the bare TiO₂ layer. This supports our previous conclusion that the eventual after-pulse decay of electrons occurs via deep trapping at intrinsic chemical or physical defects within the TiO₂ matrix. The time scale for the eventual interfacial recombination of trapped electrons with the valence band hole or porphyrin radical cation sites, process 7B and 6B in Figure 1, would appear to take place on a time scale considerably longer than that of the intrinsic decay process. This is corroborated by the results obtained by Durrant and co-workers,[27,28] who determined the charge recombination kinetics of three different sensitizers, including the porphyrin studied in this work, by monitoring the transient absorption decay of the dye radical cation, showing that recombination of the trapped electron with the oxidized dye takes place on much longer (> 100 μs) time scales. Furthermore, it is also demonstrated[27] that the decay of the electron due to recombination of trapped electrons with the dye radical cation is much stronger influenced by the illumination intensity and hence the occupancy of trap states.

Conclusions

We have applied the FP-TRMC technique to study photo-induced charge separation in bare and porphyrin-sensitized nanocrystalline TiO₂ films. This technique enables the key parameters of photovoltaic materials such as the trap density, the wavelength dependence of the charge separation efficiency, the intensity dependence of the photoconductivity and the decay kinetics to be determined in the absence of electrodes and electrolyte.

Microwave photoconductivity transients, resulting from the formation of mobile, conduction band electrons in the semiconductor have been measured on excitation with UV (300 nm)

and visible (410−700 nm) light. The product of the yield of formation of mobile charge carriers, ϕ, and the sum of their mobilities, $\Sigma\mu$, has been determined from the maximum conductance for incident light intensities varying from $\sim 10^{12}$ to $\sim 10^{16}$ photons/cm^2 per pulse.

The photoconductivity action spectrum of the coated nc-TiO$_2$ layer displays the same spectral features as those present in the optical attenuation spectrum of the film, indicating that electron injection occurs from the porphyrin S$_1$ state. The maximum value of the charge separation efficiency per photon absorbed by the porphyrin amounts to 18% on irradiation in the Soret band. The mobility and secondary interactions of electrons within the TiO$_2$ matrix are independent of whether they are formed directly by band-gap excitation or indirectly via electron injection from the antenna layer.

The initial increase in $\phi\Sigma\mu$ with intensity is explained by the equilibrium localization of electrons at (surface) trapping sites and the gradual filling of these traps as the intensity (total number of electrons formed) is increased. This effect is absent in the presence of continuous background UV illumination, which presaturates the trapping sites prior to the laser pulse. The trap-free mobility of electrons within the anatase nanoparticles is determined to be 0.034 cm^2/Vs. This corresponds to an *intraparticle* electron diffusion coefficient, $D(-)_p$, of ca. 10^{-3} cm^2/s which is an order of magnitude larger than the value of ca. 10^{-4} cm^2/s found for $D(-)_b$ in DC measurements.[20] There is almost no effect of the bias illumination for conditions of laser pulse intensity corresponding to one or more photoexcitations per particle, irrespective of the presence of adsorbed sensitizer. We conclude that equilibrium electron localization is related to a property of the whole semiconductor particle, rather than to chemical or physical surface defects since the latter is likely to be influenced by the presence of the adsorbant.

For illumination intensities corresponding to an electron occupancy exceeding 1 per TiO$_2$ nanoparticle, a decrease in photoconductivity is observed, most probably due to a decrease in the effective, intraparticulate electron mobility as a result of electrostatic charging of the particles.

The after-pulse decay of the photoconductivity, which occurs over a time scale of several microseconds, becomes faster for increasing intensity in the pulse. We explain the decrease in decay time with increasing intensity by the increased rate of diffusion through the matrix to deep defects, eventually (in the $>100\,\mu$s time domain) followed by recombination with trapped hole sites.